Mechanism and Machine Theory 78 (2014) 307–323

Contents lists available at ScienceDirect

Mechanism and Machine Theory

journal homepage: www.elsevier.com/locate/mechmt

UT hand I: A lock-based underactuated hand prosthesis

Bart Peerdeman [a,*,1], Marcello Valori [b,1], Dannis Brouwer [a], Edsko Hekman [a], Sarthak Misra [a], Stefano Stramigioli [a]

[a] University of Twente, The Netherlands
[b] Polytechnic University of Bari, Italy

ARTICLE INFO

Article history:
Received 16 July 2013
Received in revised form 24 March 2014
Accepted 28 March 2014
Available online 13 May 2014

Keywords:
Hand prosthesis
Underactuation
Joint locking
Grasping

ABSTRACT

In this paper, a new prototype underactuated hand prosthesis is presented. Its design is based on a robotic finger concept featuring tendon-pulley underactuation, joint coupling, and a series of joint locking mechanisms. The joint locks serve to actively control the degrees of freedom of the four fingers, allowing a single actuator to perform a variety of grasping motions. The thumb is separately actuated by a combination of opposition and flexion motors. Rubber fingertips add compliance to the grasp, and can be equipped with an integrated tactile sensor array. The prototype's kinematics are evaluated, and its functionality is demonstrated by performing a series of grasps. The results show that the UT Hand I provides the advantages of minimal actuation, without reducing its functionality.

1. Introduction

In recent years, several advanced myoelectric hand prostheses have become commercially available [1–3]. These hands offer a significantly higher number of degrees of freedom (DOFs) than traditional prostheses. However, despite their increased functionality, a large percentage of myoelectric prostheses still go unused by their owners [4,5].

To circumvent this problem, a list of requirements has been set up based on input by users, clinicians and engineers [5]. For the mechanical design of a hand prosthesis, these requirements can be divided into two categories:

- Anthropomorphic: the prosthesis should resemble the human hand as much as possible, in both appearance and functionality. This not only affects the size and weight of the hand, but also the fingers' dynamic behavior and thumb opposition.
- Grasping: activities of daily living for single-sided amputations almost invariably involve grasping and holding of objects with the prosthesis, while the able hand performs manipulation tasks. To this end, the prosthesis should be able to perform a variety of grasp types relevant to these activities (see Fig. 2):
  - Lateral grasp, which keeps all fingers flexed and uses the thumb to grasp flat objects
  - Cylindrical grasp, which uses all fingers and an opposed thumb to firmly grasp larger objects
  - Tripod grasp, which uses the index and middle fingers and the thumb to grasp smaller objects while keeping the ring and little fingers flexed
  - An index finger point gesture should also be supported.

Abbreviations: DIP, distal interphalangeal joint; PIP, proximal interphalangeal joint; IP, interphalangeal joint; MCP, metacarpophalangeal joint.

* Corresponding author at: Matenweg 32-104, 7522 LK Enschede, Overijssel, The Netherlands. Tel.: +31 648584257.
E-mail address: b.peerdeman@utwente.nl (B. Peerdeman).

[1] Authors 1 and 2 contributed equally to this paper and should be considered co-first authors.

http://dx.doi.org/10.1016/j.mechmachtheory.2014.03.018

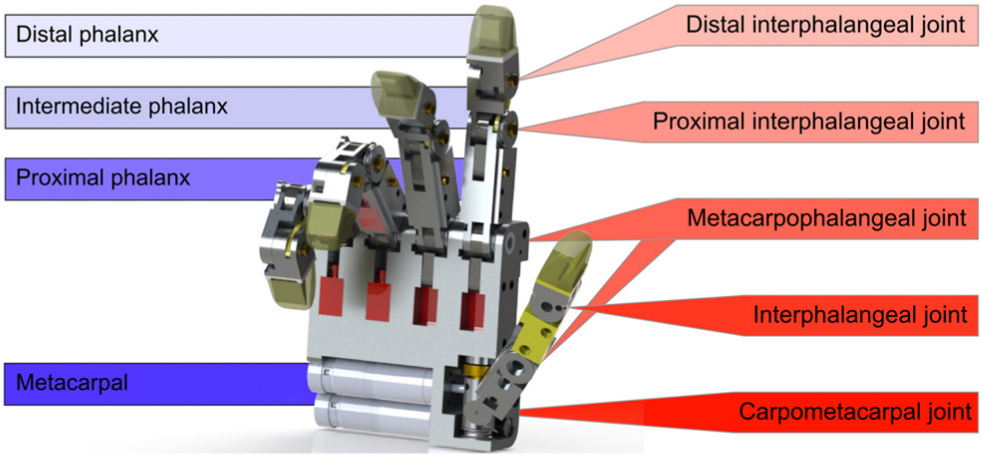

Fig. 1. A rendering of the UT Hand I prosthesis prototype, indicating phalanx and joint names.

Minimizing actuation is a crucial part of prosthesis design; a low number of actuators requires less volume and reduces weight. Underactuation has already been used in the development of several prototype hand prostheses [6–13], where it is achieved by means of many different strategies, such as:

◦ Mechanisms for rigid joint coupling [6–10]
◦ Tendon-pulley drive [11]
◦ A Geneva drive to alternately actuate different DOFs [8,10]
◦ Compliantly linking the actuation of multiple fingers [11,7,9,10]
◦ Passive, compliant joints [8,12].

However, every one of these mechanisms reduces the effective number of controllable DOFs. A system of joint locks has been developed to re-establish a measure of control over the motion of underactuated fingers [14].

In this paper, a new design for an underactuated hand prosthesis is presented: The UT Hand I (Fig. 1). The prototype implements a robotic finger concept based on ideas put forth in Wassink et al. [15]. A combination of a tendon-pulley system and four-bar linkages is used to actuate the four fingers' 12 DOFs with a single DC motor. The joint locking systems have been improved for the UT Hand I; 8 locks are installed in the palm and proximal phalanges to control the hand's grasping motions. The system also includes a 3-DOF thumb with two actuators.

The joint locking technology is the core of the underactuation strategy of this prototype. It allows a reduction in the number of continuous actuators, while maintaining the possibility of controlling different DOFs individually and adding only a small amount of weight and volume. This gives the UT Hand I an advantage with respect to many existing hand prostheses, the advertised DOFs of which often include both active and passive ones.

The design of the prototype is described in detail in Section 2. Section 3 covers the kinematic analysis of the system. In Section 4, the results of the preliminary prototype tests are shown and discussed. Section 5.1 concludes the paper.

2. Prototype concept and design

In Fig. 3, the UT Hand I is shown. The hand features the following mechanisms:

1. The hand's underactuation is obtained by implementing a single DC motor to flex all joints of the four fingers.
2. Each of the four fingers is equipped with two friction-based joint locks, actuated by small solenoids. Different grasp types are obtained by locking certain finger joints, allowing selective actuation of the unlocked joints [14].
3. In each finger, the rotation of the DIP joint is coupled to that of the PIP joint by a four-bar mechanism.

Fig. 2. Three grasp types commonly used in activities of daily living, from left to right: cylindrical, lateral, and tripod [5].

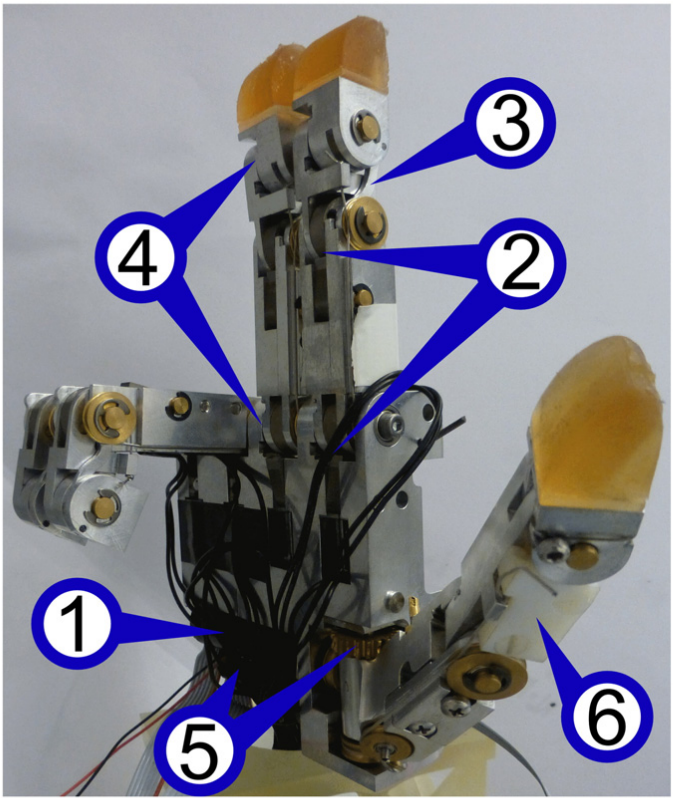

Fig. 3. The UT Hand I prosthesis prototype; 1–6 indicate relevant subsystems.

4. Extension springs are implemented to extend the fingers and maintain tension in the tendon transmission.
5. To actuate the thumb, two DC motors are used: one for flexion, and a smaller one for opposition.
6. The thumb's IP joint rotation is coupled to that of its MCP joint by a tendon coupling.

2.1. Joint locking

In Peerdeman et al., a mechanism was designed to individually lock the joints of an underactuated finger [14]. By using a friction-based self-locking principle, the mechanism shown in Fig. 4 can continuously block the rotation of an actuated joint with only a single low force solenoid actuator. These mechanisms have been implemented and tested in a two-fingered setup [16]; based on the results of those tests, several improvements have been made. Most notably, the lock's drum is coated with a layer of 10 μm silicon carbide particles embedded in nickel, which serves to increase the friction of the drum. This increase in friction

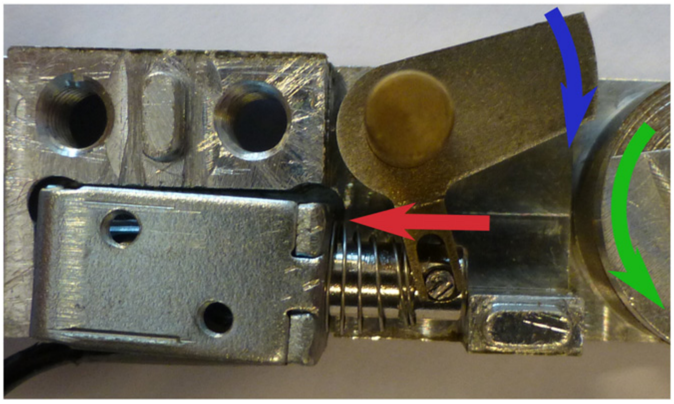

Fig. 4. The joint locking mechanism. The arrows indicate the operating direction of the solenoid (red) and pawl (blue), and the locking direction of the drum (green).

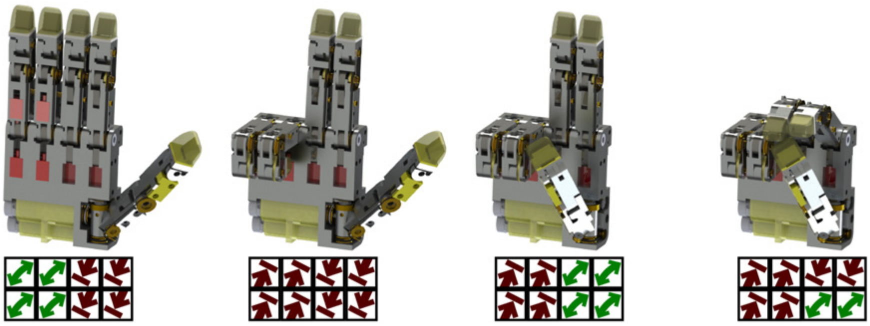

Fig. 5. The different hand configurations required for tripod grasping. The symbols show the state of all joint locks; green arrows represent unlocked joints, and red arrows indicate a locked direction. From left to right: 1: Index and middle fingers are locked in the flexion direction; little and ring fingers are fully flexed. 2: Little and ring fingers are locked in the extension direction. 3: Index and middle fingers are unlocked while thumb is brought into opposition. 4: Fingers and thumb are flexed, while locking the distal finger joints to ensure a stable grasp.

allows for a higher contact angle between the pawl and drum while keeping the self-locking property of the system intact. A higher contact angle in turn reduces the contact forces in the locking system and the compliance of the locked joints. The increased friction and contact angle of the new design also allow for a smaller solenoid actuator, reducing the general dimensions of the mechanism. In this prototype, the updated joint locks are used to control four fingers with a single actuator. Four of the locking mechanisms are integrated into the palm, and one is integrated into the proximal phalanx of each finger.

The current implementation of the joint lock is unidirectional, and therefore the desired locking direction needs to be considered for each joint. The tripod grasp requires separate extension of the index and middle fingers with regard to the ring and little fingers, which need to remain flexed while the grasp is being executed. A description of the tripod grasp and associated joint locking is shown in Fig. 5. To this end, the index and middle fingers have locks in the flexion direction, and the ring and little fingers can be locked in the extension direction. This configuration does not interfere with the cylinder and lateral grasps, and also allows the hand to perform an index finger point.

2.2. Finger design

A picture of the index finger is shown in Fig. 6, highlighting its various subsystems. The structure of the other fingers is identical, except for the orientation of the joint locking mechanism. The fingers are connected to a steel actuation tendon at the intermediate phalanx, which actuates their flexion. Extension is done by a pair of torsion springs placed in the proximal and distal joints. The DIP and PIP joints are coupled by a four-bar linkage. A tactile sensor array is placed inside the fingertip, and flexure sensors are placed on each joint to measure its rotation angle.

2.2.1. Four-bar coupling

In the fingers of the human hand, the rotation angle of the DIP joint with respect to the PIP joint is characterized by a transmission ratio of approximately 2:3 [17]. Considering this ratio, a coupling between the two joints would reduce the number of DOFs without affecting the dynamic appearance and function of the hand. Coupling the motion of multiple finger joints can be achieved in several ways, such as mechanical linkages [18,19] or tendon-pulley systems [8,11]. For the fingers of this prototype, a four-bar linkage has been chosen, as it requires little space and provides a bidirectional coupling. The structure of the linkage is shown in Fig. 7.

To determine the relative orientation of the distal phalanx, an analytical approach is used. Compared to the use of closure equations simplified by Freudenstein's equation [20], this approach serves to evaluate the mechanism's variable coupling ratio across the joint's entire range of motion. The approach is illustrated in the inset of Fig. 7; definitions of the variables used in this

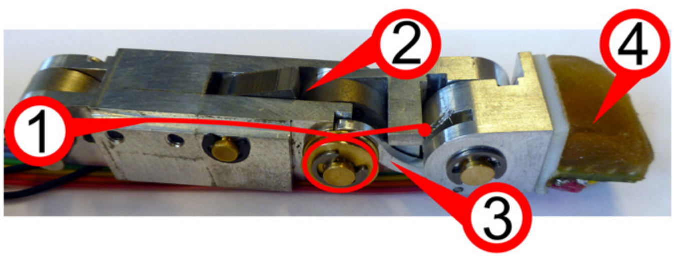

Fig. 6. The index finger and its subsystems: 1: tendon-pulley actuation, 2: joint locking mechanism, 3: four-bar coupling, and 4: tactile sensor array.

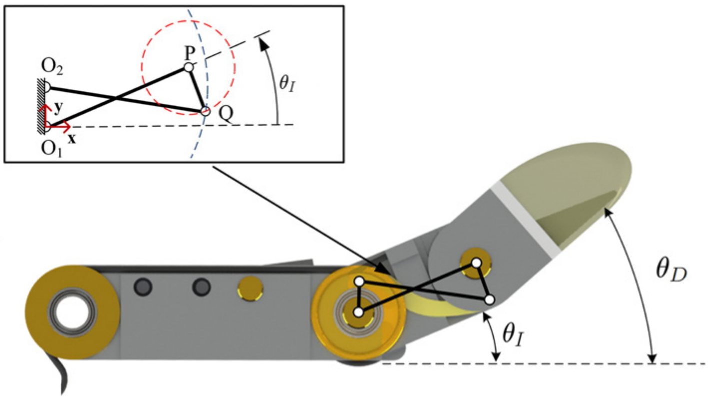

Fig. 7. The four-bar mechanism of the finger. P, Q, O_1 and O_2 indicate the positions of the mechanism's joints. The rotation angles of the intermediate ($\boldsymbol{\theta}_I$) and distal phalanges ($\boldsymbol{\theta}_D$) are indicated with respect to the proximal phalanx.

approach can be found in Table 1 in Appendix 1. With the coordinates of P being defined as $\{b_{PO_1}cos(\theta_I), b_{PO_1}\sin(\theta_I)\}^T$, the coordinates of Q can be derived from the following equations:

$$\begin{aligned}(x_Q - x_P(\theta_I))^2 + (y_Q - y_P(\theta_I))^2 &= b_{PQ}^2 \\ \left(x_Q - x_{O_2}\right)^2 + \left(y_Q - y_{O_2}\right)^2 &= b_{QO_2}^2.\end{aligned} \tag{1}$$

The analytical function $\theta_D(\theta_I)$ describing the distal phalanx's motion can then be obtained by means of Eq. (1) and the following:

$$\frac{\partial \theta_D}{\partial \theta_I} = \frac{\partial \arctan\left(\frac{y_Q - y_P}{x_Q - x_P}\right)}{\partial \theta_I}. \tag{2}$$

Due to the presence of the shaft, bearings and locking mechanism at the intermediate joint, the choice of position for the linkage joints is very restricted. The best solution for our purposes generates a slope described in Fig. 8. The distal phalanx rotation differs from the desired behavior at high angles, but this will only occur when the finger is nearly fully flexed, which will not affect the grasping action.

2.2.2. Sensors

Proper control of the hand prosthesis requires information on the pose of each finger and any contact forces applied to the fingers. This information is provided by a set of angle sensors placed on each joint, and a tactile sensor array which can be integrated into the fingertip. The tactile sensors are based on the TakkTile system [21]. The sensor consists of an array of MEMS barometers covered in a molded urethane rubber fingertip, which also serves to improve the hand's grasping performance. To determine the angle of each joint, a flexure sensor is wrapped around the outside of the joint. This provides the necessary information without requiring significant space in the finger.

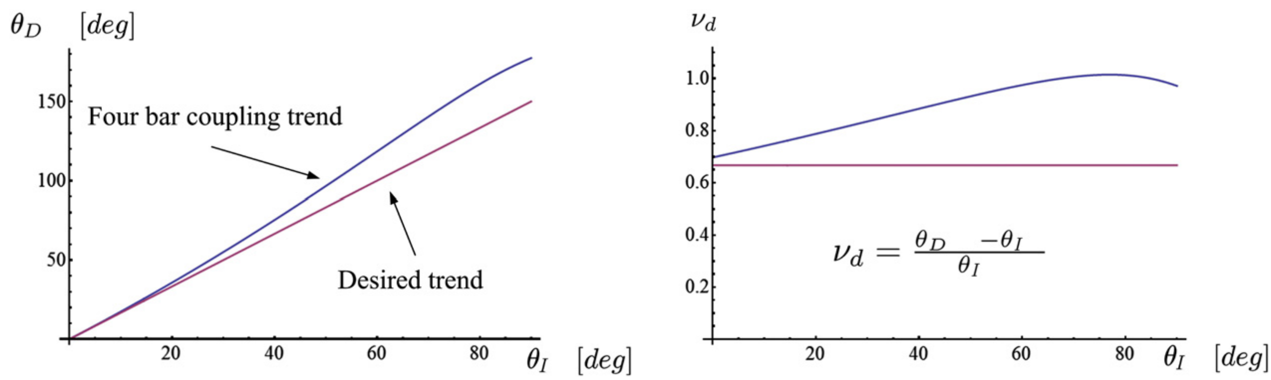

Fig. 8. The desired and actual angles of the intermediate ($\boldsymbol{\theta}_I$) and distal phalanges ($\boldsymbol{\theta}_D$) due to the four-bar mechanism.

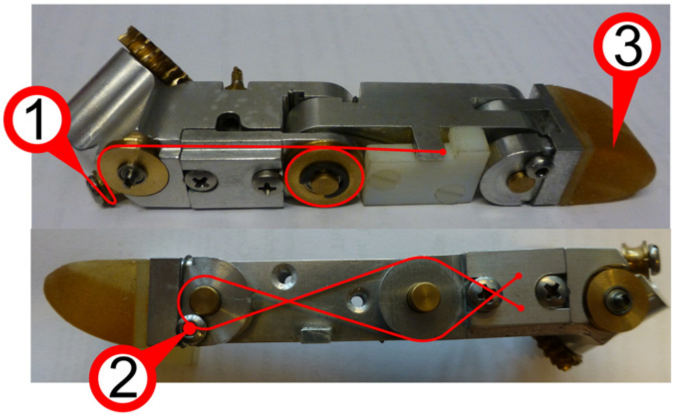

Fig. 9. The thumb and its subsystems: 1: tendon-pulley actuation, 2: tendon coupling, and 3: urethane rubber tip.

2.3. Thumb design

The structure of the thumb is shown in Fig. 9. Compared to the fingers, the most notable difference is its opposition motion. In this prototype, opposition is accomplished by placing the thumb at a 45° angle to both the other fingers and the plane of the palm. This causes the thumb itself to move along a cone centered on the shaft, approximating the opposition motion of the human hand with a single DOF.

2.3.1. Actuation

Flexion of the thumb is actuated by a single tendon connected to the thumb's proximal phalanx. This tendon has to be routed along several pulleys in order to align with the thumb's flexion plane. It should also be noted that opposition of the thumb will result in flexion of the thumb or slacking of the flexion tendon. Therefore, opposition of the thumb should be coordinated with movement of the flexion motor; this is addressed in Section 3.2. The opposition motor is only used during preshaping, and is not required to exert the higher forces involved in grasping; however, external forces due to grasping or contact with the environment require some measure of non-backdrivability in the opposition joint. Therefore, a worm wheel transmission has been placed between the thumb shaft and the opposition motor.

2.3.2. Tendon coupling

The ratio between the thumb's distal and proximal phalanges' flexion angles is different from that of the fingers. Based on the relative motion of the human thumb's joints [22], an approximate ratio of 2:1 between the prosthesis' IP and MCP thumb joints has been chosen. The combination of this transmission ratio and the spatial limits of the thumb would lead to a four-bar mechanism that reaches a singular position. Though the mechanism's behavior would be close to the desired one, a high transmission ratio is present at low flexion of the distal phalanx. Therefore, a tendon coupling has been implemented. Although such a mechanism requires additional space, this does not pose a problem as the thumb is wider than the fingers and its phalanges do not contain joint locks.

The design of the tendon coupling is shown in Fig. 10. It consists of a crossed connection of two nylon tendons, which are routed around two circular cams. The crossed cables provide a bidirectional coupling of the distal phalanx angle. The transmission ratio of the coupling is defined by the ratio $\frac{r_{MCP}}{r_{IP}}$, and can therefore be set exactly to the desired 2:1.

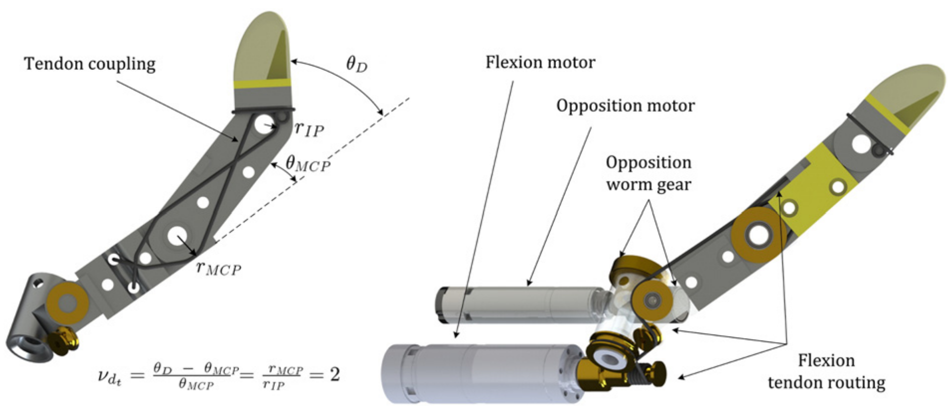

Fig. 10. A diagram of the thumb's tendon coupling, and the elements of its actuation system. For the tendon coupling, relevant angles and radii are indicated.

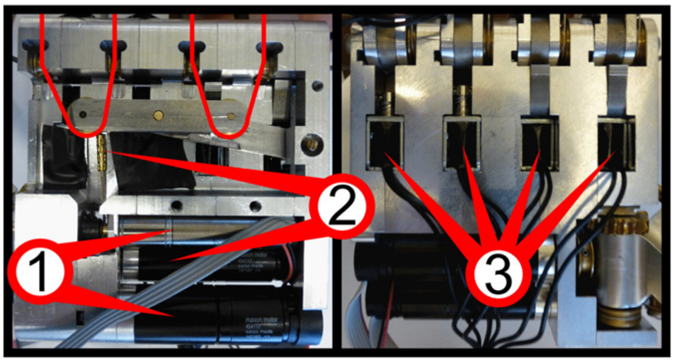

Fig. 11. The palm and its subsystems: 1: thumb actuation motors, 2: finger actuation motor and tendon-pulley linkage, and 3: joint locking mechanisms.

2.3.3. Sensors

The sensors of the thumb are identical to those of the fingers. However, the thumb can also be equipped with a socket for a BioTac sensorized fingertip [23]. This will eliminate the thumb's distal DOF, but allow for a more accurate measurement of external forces on the tip.

2.4. Palm design

As with the rest of the prototype, the design of the palm is restricted to a size similar to the human hand. The dimensions of the palm have been chosen to be 90 × 82 × 26 mm, in accordance with an average male hand [24]. The palm can be divided into several sections, housing the finger joints, thumb joint, joint locks, linkage system, and actuators. These sections are shown in Fig. 12. The palm has been manufactured in 5 parts, which are connected and aligned by two shafts running through the palm.

2.4.1. Actuation system

Due to the variety in the length of the remaining limb after a transradial amputation, most recent hand prostheses implement an actuation system that is included in the palm of the hand [6,11,7–10,12,13,25,26]. These prostheses also almost exclusively feature DC motor actuation, although actuation by means of pressurized CO_2 cartridges [26,27], monopropellant gasses [28], or shape memory alloy actuators [29] have also been investigated. In this prototype, for reasons of reliability and controllability, DC motors have been chosen over more experimental actuation methods.

The palm contains three DC motors (Maxon Motor AG, Switzerland), used to actuate the four fingers' flexion and thumb's flexion as well as the opposition of the thumb. The two flexion motors are 16 mm brushless DC motors [30], with a 157:1 planetary gearhead, whereas for opposition a 10 mm brushless DC motor [31] with a 16:1 reduction is used. The flexion motors have been chosen with regard to maximum torque and maximum velocity requirements. A 5–10 N load for each of the four fingers is considered, and 15–20 N for the thumb; for flexion velocity, complete flexion of all the fingers in 1 s was considered acceptable.

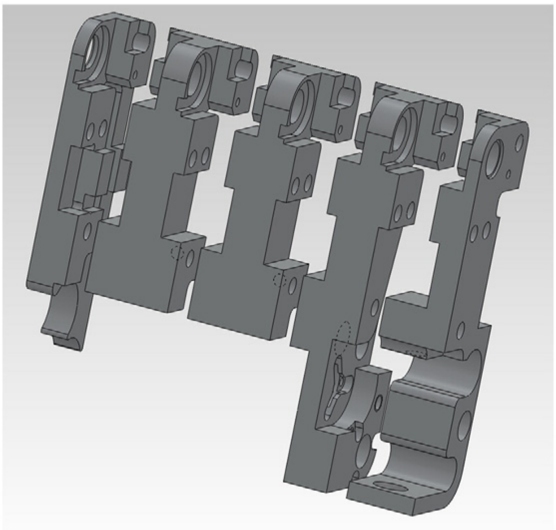

Fig. 12. The palm structure, divided into its constituent parts.

All motors are located in the lower part of the palm, in order to concentrate the hand's mass as close as possible to the hypothetical wrist. Their position optimizes the available volume; it also allows room for motion of the transmission elements (pulley tree, tendon reels and worm gear).

2.4.2. Transmission

The relative position of the fingers can vary based on the selected grasp type and the object being grasped. Therefore, the mechanism that distributes the actuator force across the four fingers needs to be adaptable. The four fingers are connected by tendons in pairs of two, each of which is actuated by a single pulley. The two pulleys are connected to a linkage, which can be seen in Fig. 11; a diagram of the actuation system is shown in Fig. 13. The linkage is actuated by a single tendon connected to the far end of the main beam. This configuration allows the pulleys to assume any relative position by rotating the beams, and distributes the actuator force evenly across the fingers. The combination of the linkage system and tendon transmission ensures the adaptability of the grasp: the linkage allows relative motion of the two pairs of fingers, and the tendons permit the two fingers of each pair to move independently. The extension springs in the DIP and MCP finger joints maintain the tendons' tension.

As already mentioned, two motors govern the thumb's motion. Thumb flexion is controlled in a similar way to finger flexion, with a single tendon on a reel connected to the motor. Thumb opposition is actuated via a worm gear transmission to ensure non-backdrivability. The positioning of the thumb shaft with respect to its actuators is shown in Fig. 10.

3. Modeling and kinematics

A kinematic analysis of the prototype is essential for the future development of its control system. The actuation systems of the fingers and the thumb will be analyzed to determine the velocities and forces that can be applied.

3.1. Fingers

Determining the motion of the four fingers with regard to the motion of their actuator can be complicated, given the nature of the tendon transmission and the adaptability of the underactuated mechanism. A diagram illustrating the situation is shown in Fig. 14. It should be noted that the actual finger joint velocities are also influenced by external forces, both of which will need to be detected by the prosthesis' sensor suite. However, the kinematics of the system are relevant to determining the desired motor velocity for different lock configurations and hand poses.

A diagram of the finger underactuation linkage in the palm is shown in Fig. 13; the symbols used in this figure are described in detail in Tables 1 and 3 in Appendix 1. To evaluate the mechanism, the total length of each of the two tendons (l_1 for the index and middle finger tendon, and l_2 for the ring and little finger tendon) can be divided into three 'control lengths': the lengths of the tendon paths in the fingers ($cl_{f1}$to cl_{f4}, from the index finger to the little finger), and the tendon paths in the palm (cl_{p1} and cl_{p2}). A row of 4 small pulleys (A–D in Fig. 13) separates the tendon paths in the palm from those in the fingers. As tendon stretching is considered to be negligible, the combination of a palm control length and its two associated finger control lengths will be constant.

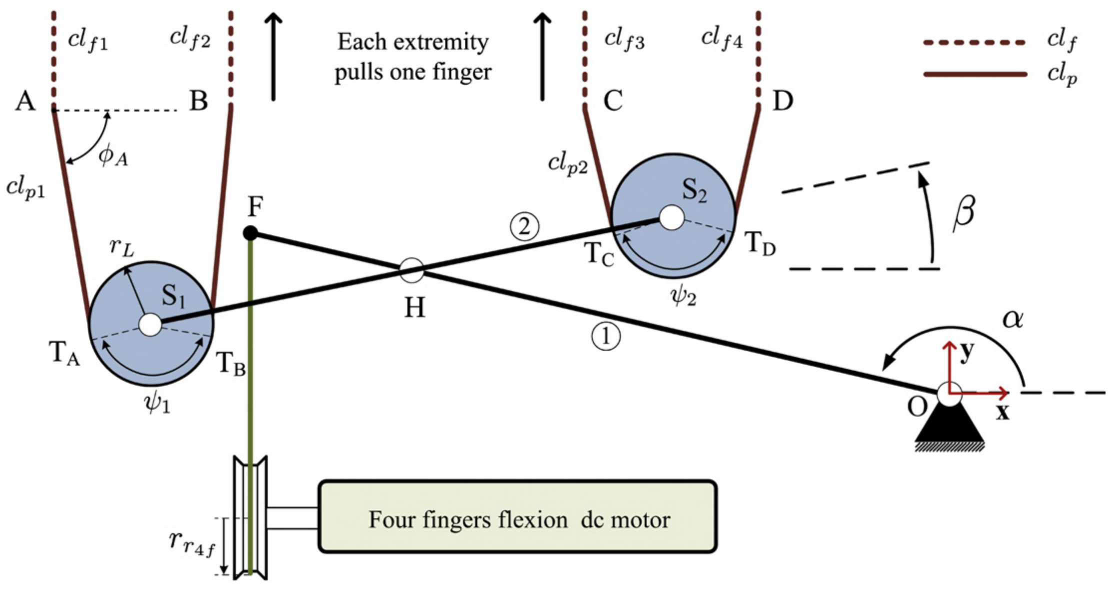

Fig. 13. A diagram of the finger actuation pulley tree linkage, indicating points, angles and lengths used in the kinematics calculations. See Tables 1 and 3 in Appendix 1 for a description of the symbols used in this figure.

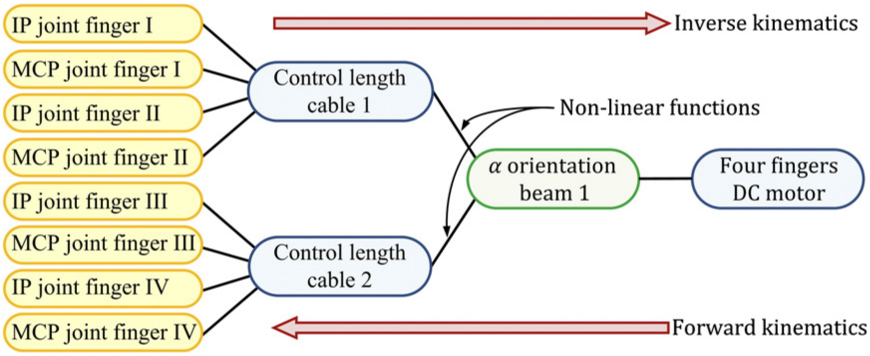

Fig. 14. A diagram of the forward and inverse kinematics of the system.

During movement of the fingers, the tendon path around the fingers is determined only by the joint angles. The tendon path in the palm is more complex, due to the floating pulleys (S_1 and S_2) in the pulley tree mechanism seen in Fig. 13. The linkage supporting the floating pulleys has 2 rotational DOFs, α and β. Thus, the location of each floating pulley is a function of the angles of both links of the linkage:

$$S_1 = b_{OH}\begin{bmatrix}\cos\alpha\\ \sin\alpha\end{bmatrix} - b_{HS_1}\begin{bmatrix}\cos\beta\\ \sin\beta\end{bmatrix}$$
$$S_2 = b_{OH}\begin{bmatrix}\cos\alpha\\ \sin\alpha\end{bmatrix} + b_{HS_2}\begin{bmatrix}\cos\beta\\ \sin\beta\end{bmatrix}. \tag{3}$$

The variation in the tangent points of each tendon with the smaller upper pulleys is considered negligible as well. The tangent points of the tendon with the floating pulleys (T_A, …, T_D) vary with the pulleys' position. This is expressed in the following equations for l_{AT_A} and T_A, in which r_L is the radius of the two pulleys:

$$l_{AT_A} = \sqrt{\|A - S_1\|^2 - r_L^2} \tag{4}$$

$$\phi_A = \arctan\left(\frac{|y_A - y_{S_1}|}{|x_A - x_{S_1}|}\right) + \arctan\left(\frac{r_L}{l_{AT_A}}\right) \tag{5}$$

$$T_A = A + \begin{bmatrix} l_{AT_A}\cos(\phi_A) \\ -l_{AT_A}\sin(\phi_A)\end{bmatrix}. \tag{6}$$

The other tangent points T_B, T_C and T_D (and corresponding lengths l_{BT_B}, l_{CT_C}, l_{DT_D}) can also be obtained in this way. The palm control lengths can then be determined by adding the lengths of tendon between the tangent points on pulleys A, …, D and the tangent points on the floating pulleys to the tendon contact arcs along the floating pulleys. The contact arc angles can be calculated as follows:

$$\psi_1 = 2\arcsin\left(\frac{\|T_A - T_B\|}{2r_L}\right), \qquad \psi_2 = 2\arcsin\left(\frac{\|T_C - T_D\|}{2r_L}\right). \tag{7}$$

This leads to the following equations for the palm control lengths:

$$cl_{p1} = \psi_1 r_L + l_{AT_A} + l_{BT_B}, \qquad cl_{p2} = \psi_2 r_L + l_{CT_C} + l_{DT_D}. \tag{8}$$

The pulley positions, and therefore the palm control lengths, vary non-linearly with regard to the linkage angles; Fig. 15 shows the relation between linkage angles and palm control lengths. The variations in the linkage angles were purposefully made as close as possible to a linear relation; the only significant exception occurs at minimal values for both α and β, which cannot occur simultaneously given the geometry of the palm linkage. This allows for the following approximation (see Table 2 in the appendix for exact values of the constants):

$$\widetilde{cl_{p1}}(\alpha,\beta) = a_1\alpha + a_2\beta + a_3 \tag{9}$$

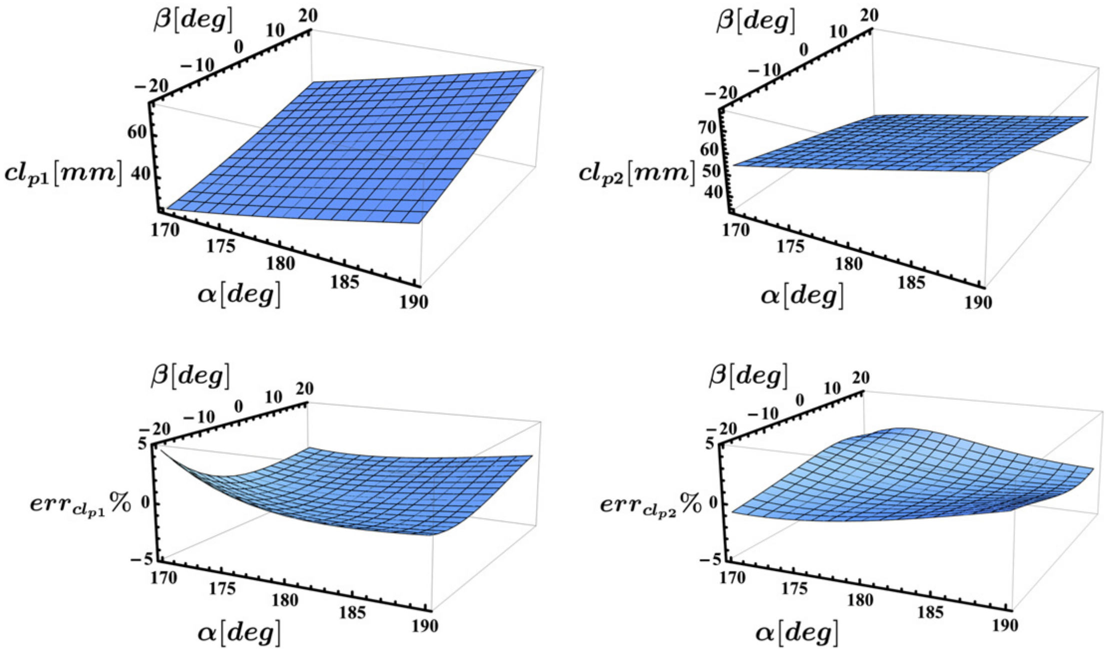

Fig. 15. Evaluation of the linkage mechanism. The top two graphs show the relationships between palm control lengths cl_{p1} and cl_{p2} and linkage angles $\boldsymbol{\alpha}$ and β. The bottom two graphs show the error percentage between the relationship above and a linear approximation.

$$\widetilde{cl_{p2}}(\alpha,\beta) = b_1\alpha + b_2\beta + b_3. \tag{10}$$

Fig. 15 also shows the error of the closest linear approximation as in Eqs. (9) and (10). The maximum error in palm tendon length between this approximation and reality is less than 1 mm. Since the variation in palm tendon length can be up to 44 or 50 mm (depending on the pulley) this is considered acceptable; closed-loop control can be used to minimize this discrepancy even further.

3.1.1. Inverse kinematics

To determine the required motor velocity to attain a desired set of finger joint velocities, the inverse kinematics of the system should be calculated. With r_J being the radius of each joint pulley, a desired change in the finger joint angles can be converted to changes in finger control lengths, and subsequently to palm control lengths as in Eq. (11). $\Delta\theta_{PIP_i}$ and $\Delta\theta_{MCP_1}$ represent the changes in the PIP and MCP joint angles of each finger.

$$\begin{aligned}\Delta cl_{p1} &= -\left(\Delta cl_{f1} + \Delta cl_{f2}\right) = r_J\left(\Delta\theta_{PIP_1} + \Delta\theta_{MCP_1} + \Delta\theta_{PIP_2} + \Delta\theta_{MCP_2}\right)\\ \Delta cl_{p2} &= -\left(\Delta cl_{f3} + \Delta cl_{f4}\right) = r_J\left(\Delta\theta_{PIP_3} + \Delta\theta_{MCP_3} + \Delta\theta_{PIP_4} + \Delta\theta_{MCP_4}\right).\end{aligned} \tag{11}$$

Using the results of Eqs. (9) and (10), the following linear approximation of the linkage angle α can be made, based on the palm control lengths cl_{p1} and cl_{p2} and constants c_1, c_2, and c_3:

$$\tilde{\alpha}\left(cl_{p1}, cl_{p2}\right) = c_1 cl_{p1} + c_2 cl_{p2} + c_3. \tag{12}$$

This also has the benefit of removing the unknown angle β from the equation, owing to the symmetric placement of the pulleys with respect to the pivot point of the main bar. $\tilde{\alpha}$ is then converted to the necessary motor output shaft rotation angle, $\varphi_{m_{4f}}$:

$$\varphi_{m_{4f}} = \frac{l_{OF}}{r_{r_{4f}}}\tilde{\alpha}. \tag{13}$$

Deriving the relations of Eqs. (11)–(13) provides the following partial Jacobian matrices:

$$\mathbf{J}_{cl}^{\theta} = \left[\frac{\partial cl_{p_i}}{\partial\theta_j}\right] = r_J\begin{bmatrix}1 & 1 & 1 & 1 & 0 & 0 & 0 & 0\\ 0 & 0 & 0 & 0 & 1 & 1 & 1 & 1\end{bmatrix} \tag{14}$$

$$\mathbf{J}_{\alpha}^{cl} = \begin{bmatrix}c_1 & c_2\end{bmatrix} \tag{15}$$

as well as the following ratio between motor velocity and change in linkage angle α:

$$\nu^{\alpha}_{m_{4f}} = \frac{b_{OF}}{r_{r_{4f}}}. \tag{16}$$

Multiplication of these relations allows us to obtain the required velocity of the motor, given the desired finger joint velocities:

$$\omega_{4f} = \overbrace{\nu^{\alpha}_{m}\mathbf{J}^{L}_{\alpha}\mathbf{J}^{\theta}_{L}}^{\mathbf{J}^{\theta_f}_{m_{4f}}}\dot{\theta}_f \tag{17}$$

$$\mathbf{J}^{\theta_f}_{m_{4f}} = \frac{b_{OF}}{r_{r_{4f}}} r_J [\, c_1 \quad c_1 \quad c_1 \quad c_1 \quad c_2 \quad c_2 \quad c_2 \quad c_2 \,]. \tag{18}$$

Assuming that the internal stiffness and friction of each finger joint is approximately equal to the others, all unlocked joints will flex at the same velocity. This velocity depends on the number of unlocked finger joints (from 0 to 4), represented by f_1 for the index and middle fingers and f_2 for the ring and little fingers. In this prototype, the ring and little fingers can only be locked in the extension direction, so f_2 is fixed at 4. The motor velocity ω_{4f} required to flex all unlocked joints at a desired velocity $\hat{\dot{\theta}}_f$ can then be derived as follows:

$$\omega_{4f} = \frac{b_{OF}}{r_{r_{4f}}} r_J (c_1 f_1 + c_2 f_2)\hat{\dot{\theta}}_f. \tag{19}$$

3.1.2. Forward kinematics

Calculation of the forward kinematics involves determining the velocity of the fingers' joints, given a certain motor velocity and status of the joint locks. As shown in Fig. 13, a decrease in length of the motor tendon will lead to an increase in the palm control lengths. The flexion of each finger joint is in turn caused by the corresponding decrease in the finger control lengths. As mentioned earlier, it is assumed that the internal frictions and stiffnesses for each joint are approximately equal, leading to an even distribution of force and velocity. Therefore, the total control length variation can be expressed as a single value l_u, which represents the control length variation for each unlocked joint. The change in l_u can then be expressed as a function of $\tilde{\alpha}$, f_1 and f_2:

$$\tilde{\alpha}(l_u) = c_1 f_1 l_u + c_2 f_2 l_u + c_3 \Rightarrow \frac{\partial \tilde{l_u}}{\partial \alpha} = \frac{1}{c_1 f_1 + c_2 f_2}. \tag{20}$$

It is then possible to express the forward Jacobian based on Eqs. (11) and (13), with $\mathbf{d}$ representing the status of all 8 joint locks (d_i is 0 for a locked joint, and 1 for an unlocked joint):

$$\tilde{\dot{\theta}}_f = \overbrace{\mathbf{d}\frac{r_{r_{4f}}}{r_J b_{OF}(c_1 f_1 + c_2 f_2)}}^{\mathbf{J}^{m_{4f}}_{\theta_f}}\omega_{m_{4f}}. \tag{21}$$

The Jacobian matrices derived in this Section illustrate the possible shortcomings of minimally actuated finger flexion. Mainly, direct control over each individual DOF is not possible, and the use of joint locking mechanisms causes a non-linear relationship between the finger joint velocities and the joint lock status variables d_i, due to their discrete nature.

3.1.3. Grasp force

The force exerted by one of the fingers on an object depends on the tendon tension (F_t), finger dimensions (l_P, l_I, and l_D), pulley radius (r_J), joint angles (θ_{MCP}, θ_{PIP}, and θ_{DIP}), and the stiffness (k) of the extension springs in the MCP and DIP joints. The torques on each finger joint can be derived from these and the coupling between the DIP and PIP joints ($\theta_{DIP} = \frac{2}{3}\theta_{PIP}$) as follows:

$$\tau_{MCP} = F_t \cdot r_J - k \cdot \theta_{MCP}, \qquad \tau_{PIP} = F_t \cdot r_J - \frac{2}{3} \cdot k \cdot \theta_{DIP}. \tag{22}$$

Based on Eq. (22) and the pose of the finger, the fingertip force ($\mathbf{F}_{MCP}$) resulting from the MCP joint torque ($\tau_{MCP} = [0{,}0{,}\tau_{MCP}]^T$) can be calculated:

$$\|\mathbf{F}_{MCP}\| = \frac{\|\tau_{MCP}\|}{\|\mathbf{l}_{MCP}\|} \tag{23}$$

$$\mathbf{l}_{MCP} = \begin{bmatrix} l_P \cos(\theta_{MCP}) + l_I \cos(\theta_{MCP} + \theta_{PIP}) + l_D \cos(\theta_{MCP} + \theta_{PIP} + \theta_{DIP}) \\ l_P \sin(\theta_{MCP}) + l_I \sin(\theta_{MCP} + \theta_{PIP}) + l_D \sin(\theta_{MCP} + \theta_{PIP} + \theta_{DIP}) \\ 0 \end{bmatrix}. \tag{24}$$

$\mathbf{F}_{MCP}$ can be determined using Eqs. (23) and (24); the direction of $\mathbf{F}_{MCP}$ is perpendicular to both τ_{MCP} and $\mathbf{l}_{MCP}$. The fingertip force resulting from the PIP joint torque can be calculated in a similar way. Assuming the motor torque to be equally divided across the four finger tendons, the average force exerted by one of the fingers during a cylinder grasp will be approximately 3.6 N.

3.2. Thumb

The kinematics of the thumb are related to its flexion and opposition movements, which have a single (effective) DOF each; as mentioned earlier, the rotation of the IP joint is compliantly coupled to that of the MCP joint. It should be noted that flexion and opposition are not completely decoupled: the flexion tendon travels around a freely rotating pulley on the thumb opposition shaft, the path of which is shortened or lengthened during opposition. Due to this, the inverse Jacobian matrix that relates flexion and opposition velocities to those of the motors is not diagonal, as expressed in Eq. (25):

$$\begin{bmatrix} \omega_{f_t} \\ \omega_{o_t} \end{bmatrix} = \overbrace{\begin{bmatrix} \frac{r_{J_t}}{r_{r_t}} & \frac{r_{S_t}}{r_{r_t}} \\ 0 & \nu_w \end{bmatrix}}^{\mathbf{J}_{m_t}^{\theta_t}} \begin{bmatrix} \dot{\theta}_{MCP_t} \\ \dot{\theta}_{OPP_t} \end{bmatrix}. \tag{25}$$

Additionally, it follows from this relation that the flexion motor could actuate both flexion and opposition degrees of freedom; this is prevented by the non-backdrivable worm wheel transmission between the opposition motor and the thumb. The forward kinematics of the thumb can be obtained by inverting Eq. (25).

3.2.1. Grasp force

The thumb tip force can be calculated by using the tendon tension and thumb pose, as demonstrated in Eqs. (22), (23) and (24). These calculations lead to an average thumb tip force of approximately 12 N.

4. Preliminary test results

To demonstrate the functionality of the underactuation mechanisms and the joint locking system, preliminary testing consists of the demonstration of three grasp types (see Fig. 2), as well as the general functionality of the joint locks.

4.1. Joint locking

To test the joint locking mechanisms in a demonstrable way, a 250 g weight is suspended from the index fingertip, as shown in Fig. 16. When the joint locks are not engaged, the finger simply flexes as the weight is released; however, the joint locks keep the finger straight when activated, even if the solenoid actuators are disabled after locking the joint.

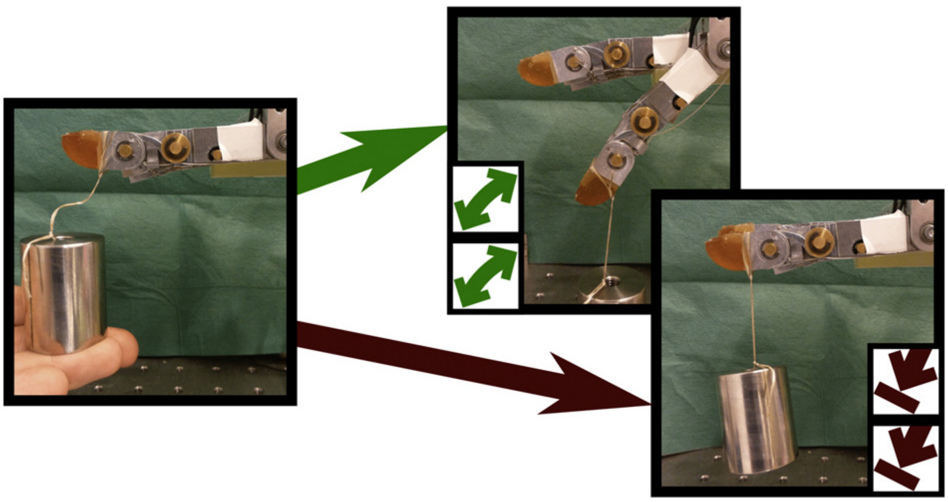

Fig. 16. A demonstration of the functionality of the joint locking mechanisms.

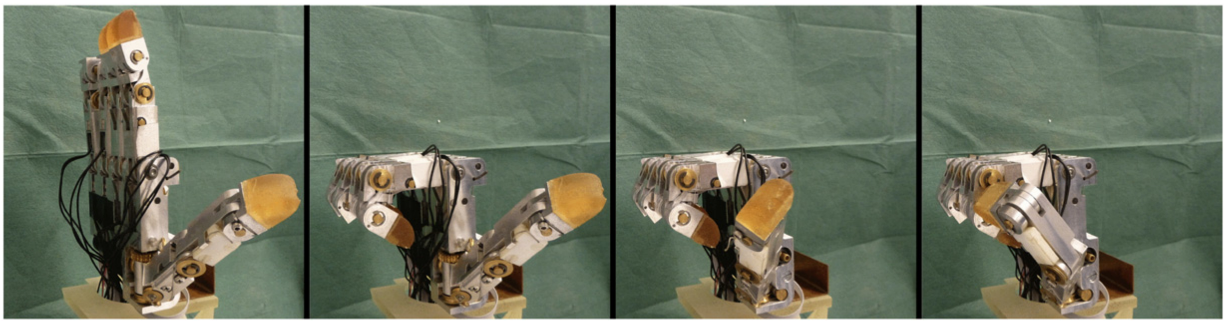

Fig. 17. A selection of frames illustrating a lateral grasp performed by the prototype.

4.2. Grasping

The various stages of each grasp are shown in Figs. 17, 18, and 19. Three videos showing the prototype performing each of these grasps are available in the electronic version of this paper. An index finger point is also executed; its result can be seen in Fig. 20.

4.2.1. Lateral grasp

Preshaping of this grasp consists of full flexion of the fingers; no joint locking is required. Once the fingers are flexed, the slightly opposed thumb can be flexed to grasp small objects between it and the side of the index finger.

4.2.2. Cylindrical grasp

Preshaping of this grasp consists of opposition of the thumb; no joint locking is required. The differences visible in the motion of the fingers are due to friction/stiffness inequalities; when the joint angles approach full flexion, or contact is established, this effect disappears. The thumb is flexed a short time after the start of finger flexion.

4.2.3. Tripod grasp

Preshaping of this grasp involves first flexing the fingers while locking the index and middle fingers' flexion. Once the ring and little fingers are fully flexed, they are locked from extending, while the index and middle fingers are unlocked. Lastly, the thumb is opposed. Flexing the fingers and thumb simultaneously, while locking the distal and intermediate joints of the index and middle fingers, will complete the grasp.

5. Discussion

The joint locking mechanisms are successful in enabling the hand's different grasping motions with minimal actuation. With the previous implementation of the joint locks in a two-fingered prototype [16], a significant degree of compliance was observed in the locked joints. The new locks' improved friction and contact angle has eliminated this compliance, and the smaller mechanism size allows all 8 MCP and PIP joints of the finger to be fitted with a lock.

The tendon-pulley underactuation linkage serves to evenly distribute the actuator force across the four fingers. The presence of small deviations in friction and stiffness on each joint can lead to an uneven flexion/extension of the fingers. The tripod and lateral grasps are executed in approximately 1 s, as per the requirements. However, during the cylinder grasp, the fingers take up to three or four seconds to fully flex. This is due to total stiffness of the fingers' extension springs being higher than expected. A set of more compliant springs, with some additional pretension, should be evaluated as an alternative. The fingertip force exerted

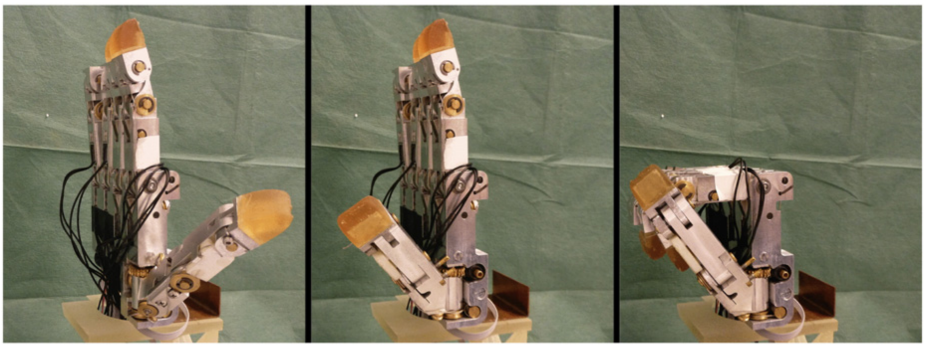

Fig. 18. A selection of frames illustrating a cylindrical grasp performed by the prototype.

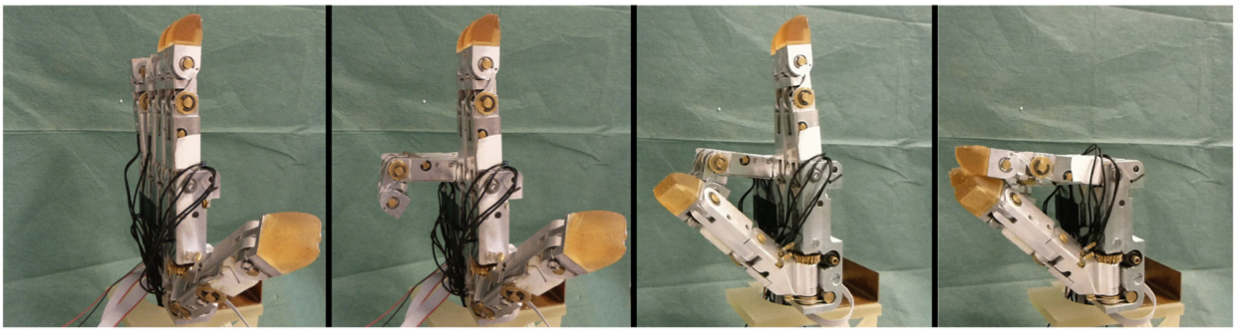

Fig. 19. A selection of frames illustrating a tripod grasp performed by the prototype.

during the cylindrical and tripod grasps was measured to be around 5 N; for the lateral grasp, 12 N was measured. While the thumb force matched the result of the force calculations, the fingertip force was somewhat higher than expected. Though these results are on the low end of the requirements, they are sufficient for the hand to establish a stable grasp.

The couplings between the distal and proximal joints of the fingers and thumb reduce the hand's DOFs to a manageable number while maintaining an anthropomorphic dynamic appearance. The compliance of the thumb tendon coupling also allows for a more flexible grasp; replacing the rigid bar in the fingers' four-bar coupling with a compliant alternative can offer such flexibility to the fingers as well. The thumb opposition worm wheel provides a non-backdrivable transmission, though the current implementation has noticeable play between the teeth. However, the existing coupling between thumb flexion and opposition helps the thumb to remain fixed while grasping.

5.1. Conclusion

This paper shows the development of the UT Hand I, a new anthropomorphic hand prosthesis prototype designed to execute several grasps relevant to activities of daily living. The hand's primary innovation is the minimal actuation system of its four fingers, the DOFs of which can be individually locked by means of miniature joint locking mechanisms. This system provides a way for modern hand prostheses to support a human-like number of controllable DOFs, while adhering to the stringent weight and size requirements imposed on anthropomorphic hands.

In order to develop a control system for the hand, its kinematics are analyzed. The transmission of actuator velocity to that of the finger joints is calculated based on the number of locked joints and current position of the fingers and pulley linkage. The required actuator velocity to attain a desired set of joint velocities is also determined, and a calculation of the fingertip forces is done.

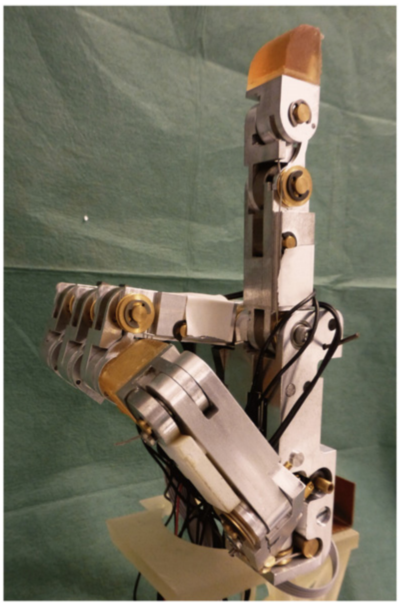

Fig. 20. The prototype performing an index finger point, by locking both joints of the index finger and flexing the fingers and thumb.

The functionality of the hand is evaluated by executing three different grasp types and an index finger point gesture. In these preliminary tests, the effectiveness of the joint locking mechanisms, joint couplings and thumb opposition is demonstrated. The combination of joint locks and underactuation proves effective in controlling the four fingers' 8 DOFs with a single actuator. Though it does not allow full simultaneous control over all DOFs, the implementation of joint locks leads to an effective variety of grasping motions and gestures, while maintaining the adaptive properties of underactuated fingers.

5.2. Future work

In future work, the control system of the UT Hand I will be developed. Using electromyographic input signals as well as the position and force sensors of the hand, the system will consist of high-level user control and low-level automatic control. The high-level controller will be based on a state machine structure, allowing several grasps and gestures to be intuitively navigated with few control signals. For the low-level controller of the hand several interaction control systems can be evaluated, such as admittance control, impedance control, and intrinsically passive control systems.

Acknowledgements

The authors would like to acknowledge Matteo Fumagalli for his assistance in getting the prototype operational.

Appendix 1. Variables and constants

The symbolic conventions adopted in the paper are made explicit here:

x	Scalar values
X	Points
$\mathbf{x}$	Vectors
$\mathbf{X}$	Matrices

The nomenclature used to express lengths between points in the kinematic equations (e.g. b_{XY} and l_{ZW}), is given by:

$$b_{XY} = |X - Y|, \qquad l_{ZW} = |Z - W|. \tag{26}$$

Table 1
Geometric values of the underactuation mechanisms in the palm, thumb and fingers.

Label	Value	Description
b_{PO_1}	20 mm	Length of one of the bars in the fingers' four-bar mechanism
b_{PQ}	6.25 mm	Length of one of the bars in the fingers' four-bar mechanism
b_{QO_2}	20.91 mm	Length of one of the bars in the fingers' four-bar mechanism
b_{OH}	41 mm	Length of one of the bars in the palm pulley linkage
b_{HS_2}	19 mm	Length of one of the bars in the palm pulley linkage
b_{OF}	57.5 mm	Length of one of the bars in the palm pulley linkage
A	$\begin{bmatrix} -71.65 \\ 15.5 \end{bmatrix}$ mm	Position of a finger alignment pulley at the top of the palm
B	$\begin{bmatrix} -53.15 \\ 15.5 \end{bmatrix}$ mm	Position of a finger alignment pulley at the top of the palm
C	$\begin{bmatrix} -30.75 \\ 15.5 \end{bmatrix}$ mm	Position of a finger alignment pulley at the top of the palm
D	$\begin{bmatrix} -12.35 \\ 15.5 \end{bmatrix}$ mm	Position of a finger alignment pulley at the top of the palm
r_L	4.25 mm	Radius of the two pulleys in the palm pulley linkage
r_J	4.85 mm	Radius of the pulleys in the joints of the four fingers
$r_{r_{4f}}$	5 mm	Radius of the reel connected to the finger flexion motor
r_{J_t}	6.75 mm	Radius of the pulley in the MCP joint of the thumb
r_{S_t}	6.5 mm	Radius of the pulley on the opposition shaft of the thumb
r_{r_t}	4 mm	Radius of the reel connected to the thumb flexion motor
l_D	45 mm	Length of the fingers' distal phalanx
l_I	20 mm	Length of the fingers' intermediate phalanx
l_P	30 mm	Length of the fingers' proximal phalanx
l_{D_t}	30 mm	Length of the thumb's distal phalanx
l_{P_t}	36.7 mm	Length of the thumb's proximal phalanx

Table 2
Mathematical constants used in the linear approximation of the palm pulley linkage kinematics.

Label	Value
a_1	76.3819 mm
a_2	34.9877 mm
a_2	−192.754 mm
b_1	66.4568 mm
b_2	−30.5868 mm
b_3	−153.817 mm
c_1	6.56165×10^{-3} mm^{-1}
c_2	7.50576×10^{-3} mm^{-1}
c_3	2.41930

Table 3
Variables used in the kinematic calculations of the palm.

Label	Description
θ_D	Angle of the finger's distal phalanx with respect to its proximal phalanx
θ_I	Angle of the finger's intermediate phalanx with respect to its proximal phalanx ($=\theta_{PIP}$)
$\theta_{PIP_1}, \ldots \theta_{PIP_4}$	PIP joint angles of the four fingers
$\theta_{MCP_1}, \ldots \theta_{MCP_4}$	MCP joint angles of the four fingers
O_1,O_2,P,Q	Joints of the finger four-bar linkage
S_1,S_2	Central points of the palm linkage pulleys
T_A,T_B,T_C,T_D	Tangent points on the palm linkage pulleys
α,β	Lagrangian parameters of the palm pulley linkage
ψ_1,ψ_2	The tendon arc angles of the two palm linkage pulleys
$l_{AT_A}, l_{BT_B}, l_{CT_C}, l_{DT_D}$	Tangent parts of the tendon control lengths
ϕ_A,ϕ_B,ϕ_C,ϕ_D	Angles of the tangent parts with respect to the line AD
l_1,l_2	Total length of the finger tendons
$\tilde{\alpha}$	Approximated linkage angle α, as per Eq. (17)
$\varphi_{m_{4f}}$	Rotation angle of the finger flexion motor shaft
$\mathbf{J}_l^\theta$	Jacobian matrix relating the angle of the finger joints to the tendon control lengths
$\mathbf{J}_\alpha^l$	Jacobian matrix relating the tendon control lengths to the palm linkage angle α
$\nu_{m_{4f}}^\alpha$	Transmission ratio between α and the finger flexion motor
$\mathbf{J}_{m_{4f}}^{\theta_f}$	Inverse Jacobian matrix for the four fingers
$\mathbf{J}_{\theta_f}^{m_{4f}}$	Forward Jacobian matrix for the four fingers
$\mathbf{J}_{m_t}^{\theta_t}$	Inverse Jacobian matrix for the thumb
f_1, f_2	Number of unlocked joints for each tendon
l_u	Variation in palm control length for each of the unlocked finger joints
$\mathbf{d}$	Vector of the joints' lock status (0 if locked, 1 if unlocked)
$\dot{\theta}_f$	Vector of the fingers' PIP and MCP joint velocities
$\dot{\theta}_{MCP_t}$	Flexion velocity of the thumb MCP joint
$\dot{\theta}_{OPP_t}$	Opposition velocity of the thumb
ω_{4f}	Rotational velocity of the finger flexion motor
ω_{f_t}	Rotational velocity of the thumb flexion motor
ω_{o_t}	Rotational velocity of the thumb opposition motor

Appendix 2. Supplementary data

Supplementary data to this article can be found online at http://dx.doi.org/10.1016/j.mechmachtheory.2014.03.018.

References

[1] Touch Bionics Inc., i-LIMB Hand.
[2] Otto Bock, Michelangelo Hand.
[3] RSLSteeper, the bebionic hand.
[4] D.J. Atkins, D.C.Y. Heard, W.H. Donovan, Epidemiologic overview of individuals with upper-limb loss and their reported research priorities, J. Prosthetics Orthot. 8 (1) (1996) 2–11.
[5] B. Peerdeman, D. Boere, H. Witteveen, R. Huis in't Veld, H. Hermens, S. Stramigioli, J. Rietman, P. Veltink, S. Misra, Myoelectric forearm prostheses: state of the art from a user requirements perspective, J. Rehabil. Res. Dev. (JRRD) 48 (6) (2011) 719–738.
[6] R. Weir, M. Mitchell, S. Clark, G. Puchhammer, M. Haslinger, R. Grausenburger, N. Kumar, R. Hofbauer, P. Kushnigg, M.E.V. Cornelius, H. Eaton, D. Wenstrand, The intrinsic hand a 22 degree-of-freedom artificial hand-wrist replacement, Proceedings of the MyoElectric Controls/Powered Prosthetics Symposium, Fredericton, Canada, 2008.

[7] D. Yang, J. Zhao, Y. Gu, X. Wang, N. Li, L. Jiang, H. Liu, H. Huang, D. Zhao, An anthropomorphic robot hand developed based on underactuated mechanism and controlled by EMG signals, J. Bionic Eng. 6 (2009) 255–263.
[8] J. Pons, E. Rocon, R. Ceres, D. Reynaerts, B. Saro, S. Levin, W. van Moorleghem, The MANUS-HAND dextrous robotics upper limb prosthesis: mechanical and manipulation aspects, Auton. Robot. 16 (2) (2004) 143–163.
[9] N. Dechev, W.L. Cleghorn, S. Naumann, Multiple finger, passive adaptive grasp prosthetic hand, Mech. Mach. Theory 36 (10) (2001) 1157–1173.
[10] J.U. Chu, D.H. Jung, Y.J. Lee, Design and control of a multifunction myoelectric hand with new adaptive grasping and self-locking mechanisms, Proceedings of the IEEE International Conference on Robotics and Automation, 2008, pp. 743–748.
[11] C. Cipriani, M. Controzzi, M.C. Carrozza, The smarthand transradial prosthesis, J. Neuroeng. Rehabil. 8 (29) (2011) 1–14.
[12] M.C. Carrozza, G. Cappiello, G. Stellin, F. Zaccone, F. Vecchi, S. Micera, P. Dario, A cosmetic prosthetic hand with tendon driven under-actuated mechanism and compliant joints: ongoing research and preliminary results, Proceedings of the 2005 IEEE International Conference on Robotics and Automation (ICRA), 2005.
[13] H. Huang, L. Jiang, D. Zhao, J. Zhao, H. Cai, H. Liu, P. Meusel, B. Willberg, G. Hirzinger, The development on a new biomechatronic prosthetic hand based on under-actuated mechanism, Proceedings of the 2006 IEEE/RSJ International Conference on Intelligent Robots and Systems, Beijing, China, 2006.
[14] B. Peerdeman, G.J. Pieterse, S. Stramigioli, J.S. Rietman, E.E.G. Hekman, D.M. Brouwer, S. Misra, Design of joint locks for underactuated fingers, Proceedings of the IEEE International Conference on Biomedical Robotics and Biomechatronics (BioRob), Rome, Italy, 2012, pp. 488–493.
[15] M. Wassink, R. Carloni, S. Stramigioli, Port-hamiltonian analysis of a novel robotic finger concept for minimal actuation variable impedance grasping, Proceedings of the IEEE International Conference on Robotics and Automation (ICRA), Anchorage, Alaska, USA, 2010, pp. 771–776.
[16] B. Peerdeman, S. Stramigioli, E. Hekman, D. Brouwer, S. Misra, Development of underactuated prosthetic fingers with joint locking and electromyographic control, Mech. Eng. Res. 3 (1) (2013) 130–142.
[17] J. Lin, Y. Wu, T.S. Huang, Modeling the constraints of human hand motion, Human Motion, Proceedings. Workshop on, 2000, 2000, pp. 121–126.
[18] S. Jung, S. Kang, I. Moon, Design of biomimetic hand prosthesis with tendon-driven five fingers, BioRob 2008. 2nd IEEE RAS & EMBS International Conference on, 2008, Biomedical Robotics and Biomechatronics, 2008, pp. 895–900.
[19] C. Light, P. Chappell, Development of a lightweight and adaptable multiple-axis hand prosthesis, Med. Eng. Phys. 22 (2000) 679–684.
[20] E.N. Haulin, A.A. Lakis, R. Vinet, Optimal synthesis of a planar four-link mechanism used in hand prosthesis, Mech. Mach. Theory 36 (11–12) (2001) 1203–1214.
[21] L.P. Jentoft, Y. Tenzer, D. Vogt, L. Jia, R.J. Wood, R.D. Howe, Flexible, Stretchable Tactile Arrays from MEMS Barometers, International Conference on Advanced Robotics (ICAR), 2013, pp. 1–6.
[22] H.-T. Lin, L.-C. Kuo, H.-Y. Liu, W.-L. Wu, F.-C. Su, The three-dimensional analysis of three thumb joints coordination in activities of daily living, Clin. Biomech. 26 (4) (2011) 371–376.
[23] N. Wettels, Biomimetic Tactile Sensor for Object Identification and Grip Control: A Multi-modal Sensor Mimicking the Human Digit, LAP Lambert Acad. Publ, 2011.
[24] B. Buchholz, T.J. Armstrong, An ellipsoidal representation of human hand anthropometry, Hum. Factors J. Hum. Factors Ergon. Soc. 33 (1991) 429–441.
[25] N.A. Andrade, G.A. Borges, F.A. de O. Nascimento, A.R.S. Romariz, A.F. da Rocha, A new biomechanical hand prosthesis controlled by surface electromyographic signals, Proceedings of the 29th Annual International Conference of the IEEE EMBS, Lyon, France, 2007.
[26] C. Pylatiuk, S. Mounier, A. Kargov, S. Schulz, G. Bretthauer, Progress in the development of a multifunctional hand prosthesis, Proceedings of the Annual International Conference of the IEEE Engineering in Medicine and Biology Society (EMBS), San Francisco, USA, 2004, pp. 4260–4263.
[27] B. Peerdeman, G. Smit, D. Plettenburg, S. Stramigioli, S. Misra, Evaluation of pneumatic cylinder actuators for hand prostheses, Proceedings of the IEEE International Conference on Biomedical Robotics and Biomechatronics (BioRob), Rome, Italy, 2012, pp. 1105–1109.
[28] S.A. Dalley, T. Wiste, T. Withrow, M. Goldfarb, Design of a multifunctional anthropomorphic prosthetic hand with extrinsic actuation, IEEE/ASME Trans. Mechatron. 14 (6) (2009) 699–706.
[29] K.T. O'Toole, M.M. McGrath, Mechanical design and theoretical analysis of a four fingered prosthetic hand incorporating embedded SMA bundle actuators, Proceedings of World Academy of Science: Engineering & Technology, Vol. 25, 2007, pp. 142–149.
[30] Maxon Motor, Re 16 dc motor.
[31] Maxon Motor, Dcx 10 dc motor.